

Flowing the Information from Shannon to Fisher: Towards the Fundamental Tradeoff in ISAC

Yifeng Xiong, *Student Member, IEEE*, Fan Liu, *Member, IEEE*, Yuanhao Cui, *Member, IEEE*, Weijie Yuan, *Member, IEEE*, and Tony Xiao Han, *Member, IEEE*

Abstract—Integrated Sensing and Communication (ISAC) is recognized as a promising technology for the next-generation wireless networks. In this paper, we provide a general framework to reveal the fundamental tradeoff between sensing and communications (S&C), where a unified ISAC waveform is exploited to perform dual-functional tasks. In particular, we define the Cramér-Rao bound (CRB)-rate region to characterize the S&C tradeoff, and propose a pentagon inner bound of the region. We show that the two corner points of the CRB-rate region can be achieved by the conventional Gaussian waveform and a novel strategy referred to as successive hypersphere coding, respectively. Moreover, we also offer our insights into transmission approaches achieving the boundary of the CRB-rate region, namely the Shannon-Fisher information flow.

Index Terms—Integrated sensing and communication, fundamental tradeoff, CRB-rate region, Shannon-Fisher information flow, successive hypersphere coding.

I. INTRODUCTION

IN an ISAC system, S&C functionalities are performed by using a single hardware platform and a common waveform over the same frequency band, which considerably improves the energy-, spectral-, and hardware efficiencies [1]–[5]. Despite the fact that S&C have long been considered as two isolated fields, they are indeed intertwined with each other as an “odd couple” in an information-theoretical sense [6].

For decades, S&C researchers are mostly working on a generic linear Gaussian model, expressed as

$$\mathbf{Y} = \mathbf{H}\mathbf{X} + \mathbf{Z}, \quad (1)$$

where \mathbf{Y} , \mathbf{H} , \mathbf{X} , and \mathbf{Z} denote the received signal, target response/communication channel, transmitted signal, and Gaussian noise, respectively, which can be in scalar, vector, or matrix forms. From the communication perspective, the basic problem is given channel \mathbf{H} to design an optimal transmission strategy \mathbf{X} that maximizes the channel capacity. On the other hand, from the sensing perspective, the basic problem is to estimate \mathbf{H} or the target parameters (e.g., amplitude, delay, angle,

and Doppler) contained in \mathbf{H} as accurate as possible, based on the knowledge of \mathbf{X} . The distinct roles of \mathbf{X} and \mathbf{H} in S&C operations lead to the interplay between S&C performance, which triggers a number of unique performance tradeoffs and design criteria [7]–[10] to the ISAC signal processing, particularly for simultaneously realizing S&C functionalities via a unified waveform. Despite that capacity characterization and parameter estimation limits have been independently investigated for S&C for years, the depiction of the inherent information-estimation tradeoff between S&C functionalities remains long standing open.

The pioneering effort to reveal the fundamental connection between information and estimation theory can be traced back to the early results on the I-MMSE equation [11], which states that the derivative of the mutual information $I(\mathbf{Y}; \mathbf{X} | \mathbf{H})$ with respect to the signal-to-noise ratio (SNR) is equal to the minimum mean squared error (MMSE) for estimating \mathbf{X} by observing \mathbf{Y} . While the I-MMSE equation implies maximizing the MMSE of \mathbf{X} also maximizes the scaling ratio of the mutual information $I(\mathbf{Y}; \mathbf{X} | \mathbf{H})$, which bridges the information theory and estimation theory, the equation itself mainly concentrates on the estimation performance of unknown data symbol \mathbf{X} rather than on the target parameters in \mathbf{H} . Consequently, the sensing performance limits for \mathbf{H} was not fully investigated. More relevant to this work, one may model the ISAC channel as a state-dependent channel, which characterizes the information-conveyed signal reflected by state-varying targets [12]. The goal for such an ISAC system is two-fold, i.e., transmitting information through such a channel while estimating its state under the minimum distortion. On top of that, a capacity-distortion (C-D) tradeoff is acquired to depict the S&C performance bounds [13]–[15]. While these studies could capture the S&C tradeoff from the information-theoretic perspective, the connections among communication capacity, target channel states, and to-be-estimated parameters in sensing tasks are still not clearly indicated.

To gain a better understanding of the interweaved S&C functionalities, in this paper, we shed light on the fundamental limits of ISAC by analyzing the tradeoff between Shannon and Fisher information, two key performance metrics at the cores of information theory and estimation theory. We consider a general point-to-point (P2P) multi-input multi-output (MIMO) system setting, where a random signal \mathbf{X} is exploited for realizing both S&C functionalities. Under such a framework, our contribution is as follows:

- We use the CRB as the performance metric for sensing, and show that its optimum is achieved when the sample

Y. Xiong is with the School of Electronics and Computer Science, University of Southampton, Southampton, SO17 1BJ, UK, and is also with the Department of Electronic and Electrical Engineering, Southern University of Science and Technology, Shenzhen 518055, China (e-mail: yx8n18@soton.ac.uk).

F. Liu and W. Yuan are with the Department of Electronic and Electrical Engineering, Southern University of Science and Technology, Shenzhen 518055, China (e-mail: liuf6@sustech.edu.cn, yuanwj@sustech.edu.cn).

Y. Cui is with the School of Information and Communication Engineering, Beijing University of Posts and Telecommunications, Beijing, China (e-mail: cuiyuanhao@bupt.edu.cn).

T. X.-Han is with Huawei Technologies Co., Ltd (e-mail: tony.hanxiao@huawei.com)

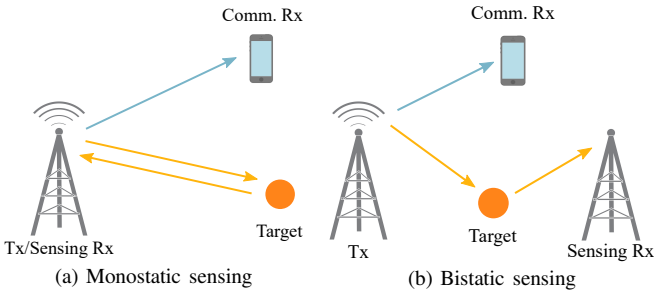


Figure 1. The ISAC scenarios considered in this paper, where the dual-functional waveform \mathbf{X} is known to the sensing receiver.

covariance matrix of \mathbf{X} is deterministic;

- We define the CRB-rate region as the set of all the achievable pairs of communication rate and sensing CRB, and show that a pentagon inner bound of the CRB-rate region can be obtained by connecting the two extreme points with a straight line;
- We derive the communication capacity for the sensing-optimal point P_{SC} , and prove that it can be achieved using a novel successive hypersphere coding strategy;
- We provide insights into the process of moving along the CRB-rate region boundary from the communication-optimal point P_{CS} to the sensing-optimal point P_{SC} , namely, the process that *information flows from Shannon to Fisher*.

To the best of our knowledge, this is the first work that addresses the fundamental tradeoff in ISAC from both information- and estimation-theoretical perspectives. Our hope is that this paper can serve as a stepping stone towards the fully characterization of the CRB-rate performance bound, as well as towards the design of bound-achieving ISAC transmission strategies.

Notations: Throughout this paper, a , \mathbf{a} , \mathbf{A} , and \mathbf{A} represent random variables (scalars), random vectors, random matrices and random sets, respectively; Their realizations, or the corresponding deterministic quantities, are denoted by a , \mathbf{a} , \mathbf{A} , and \mathbf{A} , respectively. The m -by- n matrix of zeros (resp. ones) is denoted by $\mathbf{0}_{m \times n}$ (resp. $\mathbf{1}_{m \times n}$). The m -dimensional vector of zeros (resp. ones) is denoted by $\mathbf{0}_m$ (resp. $\mathbf{1}_m$). The m -by- m identity matrix is denoted by \mathbf{I}_m . These subscripts are omitted if they are clear from the context. The Kronecker product between matrices \mathbf{A} and \mathbf{B} is denoted by $\mathbf{A} \otimes \mathbf{B}$. $\|\mathbf{x}\|_p$ denotes the l_p norm, which represents the l_2 norm by default when the subscript is omitted. The notation $\mathbb{E}_{\mathbf{x}}\{\cdot\}$ denotes the expectation with respect to \mathbf{x} , and the subscript is removed when there is no confusion. $[\cdot]^\dagger$ denotes the Moore-Penrose pseudo inverse of its argument, while $[\cdot]^H$ denotes the Hermitian transpose of its argument. $\text{tr}\{\cdot\}$ stands for the trace of a square matrix.

II. SYSTEM MODEL AND PERFORMANCE METRICS

Let us consider the general ISAC system model of

$$\mathbf{Y}_c = \mathbf{H}_c \mathbf{X} + \mathbf{Z}_c, \quad (2a)$$

$$\mathbf{Y}_s = \mathbf{H}_s \mathbf{X} + \mathbf{Z}_s, \quad (2b)$$

where $\mathbf{H}_c \in \mathbb{C}^{N_c \times M}$ and $\mathbf{H}_s \in \mathbb{C}^{N_s \times M}$ denote the communication channel and the sensing channel, respectively, $\mathbf{Y}_c \in \mathbb{C}^{N_c \times T}$ and $\mathbf{Y}_s \in \mathbb{C}^{N_s \times T}$ denote the received communication and sensing signals, respectively. $\mathbf{X} \in \mathbb{C}^{M \times T}$ denotes the transmitted dual-functional waveform employed simultaneously for communication and sensing. In this paper, we assume that \mathbf{X} is known to the sensing subsystem, but unknown to the communication receiver. This is an abstraction of the practical scenarios portrayed in Fig. 1. A more general scenario where the sensing task can be performed by the communication receiver itself will be addressed in our future works. The random matrix $\mathbf{Z}_c \in \mathbb{C}^{N_c \times T}$ denotes the received communication noise, modelled as independently and identically distributed (i.i.d.) circularly symmetric complex Gaussian random variables with zero mean, namely $\text{vec}(\mathbf{Z}_c) \sim \mathcal{CN}(0, \sigma_c^2 \mathbf{I}_{N_c \times T})$. Similarly, we also model the sensing noise \mathbf{Z}_s as $\text{vec}(\mathbf{Z}_s) \sim \mathcal{CN}(0, \sigma_s^2 \mathbf{I}_{N_s \times T})$. The communication subsystem aims for transmitting as much information as possible (reliably) to the receiver, while the sensing subsystem aims for estimating the sensing parameters $\boldsymbol{\eta} \in \mathbb{R}^K$ satisfying

$$\mathbf{H}_s = g(\boldsymbol{\eta})$$

to the highest possible accuracy, where $g(\cdot)$ is an injective mapping from \mathbb{R}^K to $\mathbb{C}^{N_s \times M}$. We limit the average power of each transmitted symbol to be P_T , hence we have

$$\text{tr}\{\tilde{\mathbf{R}}_{\mathbf{X}}\} = \mathbb{E}_{\mathbf{X}}\{\text{tr}\{\mathbf{R}_{\mathbf{X}}\}\} = P_T M, \quad (3)$$

where $\tilde{\mathbf{R}}_{\mathbf{X}} := \mathbb{E}_{\mathbf{X}}\{\mathbf{R}_{\mathbf{X}}\}$ denotes the covariance matrix of \mathbf{X} , with $\mathbf{R}_{\mathbf{X}} := T^{-1} \mathbf{X} \mathbf{X}^H$ representing the sample covariance matrix.

The performance of the communication subsystem is conventionally characterized by the achievable rate (under certain design constraints), which can be expressed as

$$R_{\mathcal{F}} = \max_{p(\mathbf{X})} T^{-1} I(\mathbf{Y}_c; \mathbf{X}), \quad \text{s.t. } p(\mathbf{X}) \in \mathcal{F}, \quad (4)$$

where $I(\mathbf{Y}_c; \mathbf{X})$ denotes the mutual information between \mathbf{Y}_c and \mathbf{X} , and \mathcal{F} denotes the feasibility region of $p(\mathbf{X})$ determined by the design constraints. The performance of the sensing subsystem is typically characterized by the estimation mean-squared error (MSE) of the parameters $\boldsymbol{\eta}$, given by

$$\text{MSE}_{\boldsymbol{\eta}}(\hat{\boldsymbol{\eta}}) := \mathbb{E}_{\mathbf{X}, \hat{\boldsymbol{\eta}}}\{\|\boldsymbol{\eta} - \hat{\boldsymbol{\eta}}\|^2\}. \quad (5)$$

However, this metric depends on the specific choice of the estimator $\hat{\boldsymbol{\eta}}$, which hinders the essential relationship between the sensing performance and the design of $p(\mathbf{X})$. To this end, we consider the CRB, which constitutes a lower bound for the MSE of unbiased estimators [16, Chap. 3], taking the following form:

$$\text{MSE}_{\boldsymbol{\eta}}(\hat{\boldsymbol{\eta}}) \geq \mathbb{E}_{\mathbf{X}}\{\text{tr}\{\mathbf{J}_{\boldsymbol{\eta}}^{-1}\}\}, \quad (6)$$

where $\mathbf{J}_{\boldsymbol{\eta}}$ denotes the Fisher information matrix (FIM) of $\boldsymbol{\eta}$ given by

$$\mathbf{J}_{\boldsymbol{\eta}} := \mathbb{E}_{\mathbf{Y}_s | \mathbf{X}} \left\{ \frac{\partial \log p_{\mathbf{Y}_s | \mathbf{X}}(\mathbf{Y}_s | \mathbf{X}; \boldsymbol{\eta})}{\partial \boldsymbol{\eta}} \frac{\partial \log p_{\mathbf{Y}_s | \mathbf{X}}(\mathbf{Y}_s | \mathbf{X}; \boldsymbol{\eta})}{\partial \boldsymbol{\eta}^T} \right\}.$$

It is well-known that certain practical estimators (e.g. the maximum likelihood (ML) estimator) are capable of achieving

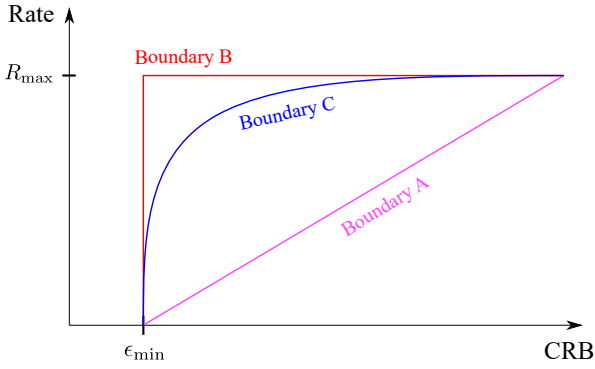


Figure 2. Graphical illustration of various possible CRB-rate regions.

the CRB when the SNR is sufficiently high [16, Chap. 7]. In light of this, in this paper, we choose the CRB of η , namely

$$\epsilon_\eta := \mathbb{E}_{\mathbf{X}} \left(\text{tr} \{ \mathbf{J}_\eta^{-1} \} \right), \quad (7)$$

as the metric of sensing accuracy.

To reveal the fundamental S&C performance tradeoff, we define the CRB-rate region, which is the set of all feasible ordered pairs (ϵ, R) , where R and ϵ are the communication rate and the sensing CRB, respectively. Typically, we are interested in the boundary of the CRB-rate region, which may be viewed as the Pareto front constituted by all optimal performance tradeoffs. To provide further intuitions about the boundary, we portray some conceptual CRB-rate regions in Fig. 2. Specifically, the point $(\epsilon_{\min}, 0)$ represents the minimum achievable sensing MSE regardless of the communication performance, while the point $(+\infty, R_{\max})$ represents the maximum achievable rate regardless of the sensing performance. The boundary A may be seen in scenarios where the integration of sensing and communication does not provide additional performance gain (but we have some *a priori* knowledge about the sensing parameters, hence the maximum CRB is not infinity), while the boundary B may be seen in idealistic scenarios where both sensing and communication performance can achieve their optimum without eroding the other. In most practical scenarios, the boundary of CRB-rate regions may have a similar shape as that of the boundary C.

III. CRB-RATE REGION ANALYSIS

In this section, we characterize the generic shape of the CRB-rate region.

A. Generic Inner Bound

Before delving into details, we first give a general description of an inner bound of the region as follows.

Proposition 1 (Pentagon Inner Bound): The convex hull of the points

$$(+\infty, 0), (+\infty, R_{\max}), (\epsilon_{\min}, 0), \quad (8a)$$

$$P_{\text{SC}} := (\epsilon_{\min}, R_1), P_{\text{CS}} := (\epsilon_1, R_{\max}) \quad (8b)$$

constitutes an inner bound of the CRB-rate region, where

$$\begin{aligned} \epsilon_1 &:= \min_{p(\mathbf{X})} \epsilon_\eta, \text{ s.t. } T^{-1}I(\mathbf{Y}_c; \mathbf{X}) = R_{\max}, \\ R_1 &:= \max_{p(\mathbf{X})} T^{-1}I(\mathbf{Y}_c; \mathbf{X}), \text{ s.t. } \epsilon_\eta = \epsilon_{\min}. \end{aligned} \quad (9)$$

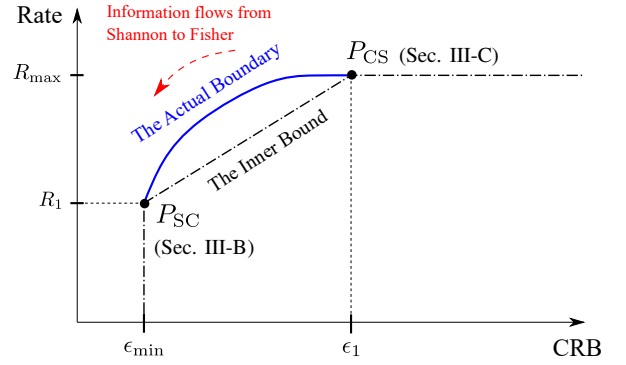


Figure 3. The pentagon inner bound of CRB-rate regions.

Proof: The points in (8a) and (8b) are obviously achievable (but note that in certain scenarios we may have $R_1 = 0$ or $\epsilon_1 = \infty$). The line segment connecting P_{SC} and P_{CS} can be achieved by using the celebrated time-sharing strategy [17, Chap. 4], namely applying the strategy corresponding to P_{SC} with probability p_1 , while applying the strategy corresponding to P_{CS} with probability $1 - p_1$. Hence the proof is completed. \square

According to Proposition 1, in general, CRB-rate regions take the form illustrated in Fig. 3. Naturally, a detailed characterization of the points P_{SC} and P_{CS} is desired. To achieve this, we first take a little detour, and derive the general form of the FIM as follows.

Proposition 2: The FIM of η takes the following form

$$\mathbf{J}_\eta = \frac{2T}{\sigma_s^2} \sum_{i=1}^{N_s} \text{Re} \{ \mathbf{F}_i \mathbf{R}_\mathbf{X} \mathbf{F}_i^H \}, \quad (10)$$

where each $\mathbf{F}_i \in \mathbb{C}^{K \times M}$ is related to a submatrix of $\mathbf{F} := \frac{\partial \mathbf{h}_s}{\partial \boldsymbol{\eta}} \in \mathbb{C}^{K \times 2N_s M}$, satisfying

$$\mathbf{F} = [\mathbf{F}_1 \dots, \mathbf{F}_{N_s}, \mathbf{F}_1^*, \dots, \mathbf{F}_{N_s}^*],$$

with $\mathbf{h}_s := [\text{vec}(\mathbf{H}_s^T)^T, \text{vec}(\mathbf{H}_s^T)^H]^T$.

Proof: Please refer to Appendix A. \square

Using Proposition 2, we may characterize the minimum achievable CRB as follows.

Corollary 1: The minimum achievable CRB ϵ_{\min} is achieved when the sample covariance matrix $\mathbf{R}_\mathbf{X}$ is deterministic, namely when $\mathbf{R}_\mathbf{X} = \tilde{\mathbf{R}}_\mathbf{X}$, and hence may be obtained by solving the following optimization problem

$$\begin{aligned} \min_{\tilde{\mathbf{R}}_\mathbf{X}} \text{tr} \left\{ \left(\sum_{i=1}^{N_s} \text{Re} \{ \mathbf{F}_i \tilde{\mathbf{R}}_\mathbf{X} \mathbf{F}_i^H \} \right)^{-1} \right\}, \\ \text{s.t. } (3), \tilde{\mathbf{R}}_\mathbf{X} \succeq \mathbf{0}, \tilde{\mathbf{R}}_\mathbf{X} = \tilde{\mathbf{R}}_\mathbf{X}^H. \end{aligned} \quad (11)$$

Proof: Using the Jensen's inequality, we obtain

$$\begin{aligned} \epsilon_\eta &= \mathbb{E}_{\mathbf{X}} \left(\text{tr} \{ \mathbf{J}_\eta^{-1} \} \right) \\ &\geq \text{tr} \{ (\mathbb{E}_{\mathbf{X}} \mathbf{J}_\eta)^{-1} \} \\ &= \frac{\sigma_s^2}{2T} \text{tr} \left\{ \left(\sum_{i=1}^{N_s} \text{Re} \{ \mathbf{F}_i \tilde{\mathbf{R}}_\mathbf{X} \mathbf{F}_i^H \} \right)^{-1} \right\}. \end{aligned} \quad (12)$$

Note that the equality is achieved when $\mathbf{R}_\mathbf{X} = \tilde{\mathbf{R}}_\mathbf{X}$, which completes the proof. \square

B. Point P_{SC} -Achieving Strategy

In general, the optimization problem (11) has to be solved on a case-by-case basis. Considering the limited scope of this paper, we defer the discussion of the detailed structure of the optimal solution to our future works, and simply denote the optimal covariance matrix as $\tilde{\mathbf{R}}_{\mathbf{X}}^{\text{SC}}$. In fact, this is sufficient for us to provide a generic characterization of the point P_{SC} in the high-SNR regime, as detailed in the following proposition.

Proposition 3 (Sensing-limited High-SNR Capacity): In the high-SNR regime, namely when $P_{\text{T}}/\sigma_c^2 \rightarrow \infty$, the rate R_1 can be expressed as

$$R_1 = \sum_{i=1}^{M_{\text{SC}}} \left(1 - \frac{2i-1}{2T}\right) \log(\lambda_i/\sigma_c^2) + c + O(\sigma_c^2), \quad (13)$$

where λ_i denotes the i -th largest eigenvalue of the matrix

$$\mathbf{G}_{\text{SC}} = \mathbf{H}_c \tilde{\mathbf{R}}_{\mathbf{X}}^{\text{SC}} \mathbf{H}_c^{\text{H}},$$

M_{SC} denotes the rank of \mathbf{G}_{SC} , while c is a constant with respect to the SNR P_{T}/σ_c^2 , and is finite as $T \rightarrow \infty$, given by

$$c = M_{\text{SC}} \left(1 - \frac{M_{\text{SC}}}{2T}\right) \log \pi T + M_{\text{SC}} \log 2 - \sum_{i=1}^{M_{\text{SC}}} \sum_{j=1}^{T-i} \log j.$$

Proof: Please refer to Appendix B. \square

Proposition 3 also enables us to propose a scheme that asymptotically achieves the point P_{SC} in the high-SNR regime, as given in the following corollary.

Corollary 2 (Successive Hypersphere Coding Achieves Point P_{SC}): In the high-SNR regime, the rate R_1 may be asymptotically achieved by a waveform \mathbf{X}_{SC} generated as follows:

$$\mathbf{X}_{\text{SC}} = \sqrt{T} \mathbf{H}_c^{\dagger} \tilde{\mathbf{U}} \tilde{\Sigma} \mathbf{Q}, \quad (14)$$

where \mathbf{H}_c^{\dagger} denotes the Moore-Penrose pseudo-inverse of \mathbf{H}_c , $\tilde{\mathbf{U}}$ contains the first M_{SC} columns of \mathbf{U} given by the eigen-decomposition of \mathbf{G}_{SC}

$$\mathbf{G}_{\text{SC}} = \mathbf{U} \Lambda \mathbf{U}^{\text{H}}, \quad (15)$$

$\tilde{\Sigma} = \text{diag}\{\sigma_1, \dots, \sigma_{M_{\text{SC}}}\}$, $\sigma_i = \sqrt{\lambda_i}$, and $\mathbf{Q} \in \mathbb{C}^{M_{\text{SC}} \times T}$ contains the modulated symbols, constructed according to a procedure that will be referred to as ‘‘successive hypersphere coding’’, detailed as follows:

- 1) Generate the first row $\mathbf{q}_1 \sim \mathcal{U}(\mathbb{C}^T)$, where $\mathcal{U}(\mathbb{C}^T)$ is the uniform distribution on the unit-norm sphere in \mathbb{C}^T ;
- 2) For $i = 2, \dots, M_{\text{SC}}$, generate $\tilde{\mathbf{q}}_i \sim \mathcal{U}(\mathbb{C}^{T-i+1})$, and obtain the i -th row \mathbf{q}_i according to $\mathbf{q}_i = \tilde{\mathbf{q}}_i \mathbf{Q}_{i-1}^{\perp}$, where $\mathbf{Q}_{i-1}^{\perp} \in \mathbb{C}^{(M_{\text{SC}}-i+1) \times T}$ contains $(M_{\text{SC}} - i + 1)$ rows forming an orthonormal basis of the null space of the matrix $\mathbf{Q}_{i-1} = [\mathbf{q}_1^{\text{T}}, \dots, \mathbf{q}_{i-1}^{\text{T}}]$.

Proof: Please refer to Appendix C. \square

Remark 1 (Successive Hypersphere Coding as Resource Allocation): It is well-known that in the conventional communication-only scenario, the capacity is achieved using the so-called ‘‘water-filling’’ strategy [18, Sec. 9.4], which allocates more power (hence higher rate) to sub-channels having higher SNR. However, in ISAC, in order to achieve P_{SC} , the power allocation strategy (characterized by $\tilde{\mathbf{R}}_{\mathbf{X}}^{\text{SC}}$) is fixed. Nevertheless, we may still assign higher rate to the

subspaces having higher SNR (corresponding to larger singular values σ_i), by allocating more degrees of freedoms in \mathbf{Q} to these subspaces. In light of this, successive hypersphere coding may be viewed as a resource allocation strategy, which sends symbols chosen from higher-dimensional hyperspheres in subspaces corresponding to larger singular values.

C. Point P_{CS} -Achieving Strategy

In contrast to that of achieving point P_{SC} , the strategy of achieving point P_{CS} is well-known in the literature [19]. Specifically, we may simply employ the capacity-achieving strategy in the communication-only scenario, which gives the maximum achievable rate

$$\begin{aligned} R_{\text{max}} &= \max_{\tilde{\mathbf{R}}_{\mathbf{X}}} \log |\mathbf{I} + \sigma_c^{-2} \mathbf{H}_c \tilde{\mathbf{R}}_{\mathbf{X}} \mathbf{H}_c^{\text{H}}|, \text{ s.t. (3)}, \\ &= \log |\mathbf{I} + \sigma_c^{-2} \mathbf{H}_c \tilde{\mathbf{R}}_{\mathbf{X}}^{\text{CS}} \mathbf{H}_c^{\text{H}}|, \end{aligned} \quad (16)$$

where the maximization with respect to $\tilde{\mathbf{R}}_{\mathbf{X}}$ can be carried out using water filling [18, Sec. 9.4], and each column \mathbf{x}_i in the P_{CS} -achieving \mathbf{X} (denoted by \mathbf{X}_{CS} following the circularly symmetric complex Gaussian distribution $\mathcal{CN}(\mathbf{0}, \tilde{\mathbf{R}}_{\mathbf{X}}^{\text{CS}})$). Then, the communication-limited minimum CRB is given by

$$\epsilon_1 = \frac{\sigma_s^2}{2T} \mathbb{E} \left\{ \text{tr} \left[\left(\sum_{i=1}^{N_s} \text{Re}\{\mathbf{F}_i \mathbf{R}_{\mathbf{X}}^{\text{CS}} \mathbf{F}_i^{\text{H}}\} \right)^{-1} \right] \right\}. \quad (17)$$

IV. DISCUSSIONS

In this section, we discuss the intuitions and implications of the results presented in Section III.

First, let us compare R_{max} with R_1 . In the high-SNR regime, according to (16), R_{max} is approximately given by

$$R_{\text{max}} \approx \sum_{i=1}^{M_{\text{CS}}} \log(\tilde{\lambda}_i/\sigma_c^2), \quad (18)$$

where M_{CS} denotes the rank of $\mathbf{H}_c \tilde{\mathbf{R}}_{\mathbf{X}}^{\text{CS}} \mathbf{H}_c^{\text{H}}$ (which equals to the rank of \mathbf{H}_c in the high-SNR regime), and $\tilde{\lambda}_i$ denotes the i -th largest eigenvalue of $\mathbf{H}_c \tilde{\mathbf{R}}_{\mathbf{X}}^{\text{CS}} \mathbf{H}_c^{\text{H}}$. This approximation implies that the number of communication degrees of freedom (DoFs) is M_{CS} . By contrast, according to (13), the sensing-limited rate R_1 in the high-SNR regime can be asymptotically bounded as

$$R_1 \geq \left(1 - \frac{M_{\text{SC}}}{2T}\right) \sum_{i=1}^{M_{\text{SC}}} \log(\lambda_i/\sigma_c^2), \quad (19)$$

$$R_1 \leq M_{\text{SC}} \left(1 - \frac{M_{\text{SC}}}{2T}\right) \log(\lambda_1/\sigma_c^2),$$

which implies that the number of communication DoFs at the point P_{SC} is $M_{\text{SC}} \left(1 - \frac{M_{\text{SC}}}{2T}\right)$. Hence we may define the *DoF efficiency* at point P_{SC} as

$$\zeta_{\text{SC}} := \frac{M_{\text{SC}}}{M_{\text{CS}}} \left(1 - \frac{M_{\text{SC}}}{2T}\right). \quad (20)$$

From (20) we observe that the DoF efficiency at point P_{SC} is determined both by the *communication subspace overlap coefficient* $\alpha_{\text{SC}} = M_{\text{SC}}/M_{\text{CS}}$ and by the *block length* T of the

dual-function waveform \mathbf{X} , which will be discussed in more detail in the following subsections.

Next, let us compare ϵ_{\min} with ϵ_1 . From (12) and (17), we observe that ϵ_1 may be rewritten as

$$\epsilon_1 = \frac{\sigma_s^2}{2T\beta_{\text{CS}}} \text{tr} \left\{ \left(\sum_{i=1}^{N_s} \text{Re}\{\mathbf{F}_i \tilde{\mathbf{R}}_{\mathbf{X}} \mathbf{F}_i^{\text{H}}\} \right)^{-1} \right\}, \quad (21)$$

where $\beta_{\text{CS}} = \frac{\text{tr}\{(\sum_{i=1}^{N_s} \text{Re}\{\mathbf{F}_i \tilde{\mathbf{R}}_{\mathbf{X}}^{\text{SC}}\})^{-1}\}}{\mathbb{E}\{\text{tr}\{(\sum_{i=1}^{N_s} \text{Re}\{\mathbf{F}_i \mathbf{R}_{\mathbf{X}}^{\text{CS}} \mathbf{F}_i^{\text{H}}\})^{-1}\}}}$ is the *sensing subspace centrality*. We will provide more insights of this quantity in Sec. IV-A.

A. The Shannon-Fisher Tradeoff: Information Flow on the Boundary of the CRB-Rate Region

In this subsection, we elaborate on the communication subspace overlap coefficient and the sensing subspace centrality. To this end, we may define the *communication subspace* as $\text{Col}(\mathbf{H}_c)$, and define the *sensing subspace* as $\text{Col}(\sum_{i=1}^{N_s} \mathbf{F}_i^{\text{H}} \mathbf{F}_i)$. Hence we may formally define the communication subspace overlap coefficient between a waveform \mathbf{X} (characterized by the corresponding $\tilde{\mathbf{R}}_{\mathbf{X}}$) and the communication subspace as

$$\alpha(\tilde{\mathbf{R}}_{\mathbf{X}}) = \frac{\text{rank}(\mathbf{H}_c \tilde{\mathbf{R}}_{\mathbf{X}} \mathbf{H}_c^{\text{H}})}{\text{rank}(\mathbf{H}_c \mathbf{H}_c^{\text{H}})}, \quad (22)$$

where the denominator is the dimensionality of the communication subspace, while the numerator may be viewed as the dimensionality of the overlap between the communication subspace and $\text{Col}(\tilde{\mathbf{R}}_{\mathbf{X}})$. As for the sensing subspace centrality, it may be formally defined as

$$\beta_{\mathbf{X}} = \frac{\text{tr}[(\sum_{i=1}^{N_s} \text{Re}\{\mathbf{F}_i \tilde{\mathbf{R}}_{\mathbf{X}}^{\text{SC}} \mathbf{F}_i^{\text{H}}\})^{-1}]}{\mathbb{E}\{\text{tr}[(\sum_{i=1}^{N_s} \text{Re}\{\mathbf{F}_i \mathbf{R}_{\mathbf{X}} \mathbf{F}_i^{\text{H}}\})^{-1}]\}}. \quad (23)$$

We observe that β may be interpreted as a metric of centrality in the sensing subspace, since \mathbf{X} has to be close to all \mathbf{F}_i 's (in terms of $\text{tr}\{\mathbf{X}^{\text{H}} \mathbf{F}_i\}$) in order to achieve a high β .

As we moving along the boundary of the CRB-rate region from P_{CS} to P_{SC} , the communication subspace overlap coefficient gradually decreases from 1 to $M_{\text{SC}}/M_{\text{CS}}$, while the sensing subspace centrality increases from its minimum to 1, which corresponds to the process that the energy of the transmitted waveform gradually flows from the communication subspace to the sensing subspace. Consequently, the Shannon information that the waveform carries decreases, but the Fisher information that could be extracted from the received signal increases. This may be viewed as the process that the information flows from Shannon to Fisher.

B. The Finite Block Length Issue: Random vs. Deterministic

Corollary 1 provides another important insight into the fundamental S&C performance tradeoff. Intuitively, to obtain a higher communication rate, one should modulate as much information as possible onto the carrier signal, hence the transmitted waveform should be ‘‘as random as possible’’. However, Corollary 1 tells us that to achieve the optimal sensing performance, the transmitted waveform has to be deterministic to a degree, in the sense that its sample covariance

matrix should be deterministic. In general, this would sacrifice some DoFs which could have otherwise been exploited for communication, hence leads to a tradeoff between communication rate and sensing accuracy.

The above-mentioned DoF penalty of achieving the optimal sensing performance is quantified by the term $(1 - M_{\text{SC}}/2T)$ in (20), which is less than 1 as long as T is finite. When the block length T is sufficiently long, the random vs. deterministic tradeoff becomes less severe, since even a communication-optimal Gaussian waveform \mathbf{X} would have asymptotically orthogonal rows as $T \rightarrow \infty$ [20].

V. CONCLUSIONS

In this paper, we have proposed a general framework for the analysis of the S&C performance tradeoff. In particular, we have introduced the CRB-rate region for characterizing the S&C tradeoff, and showed that it has a pentagon inner bound obtained by connecting the communication-optimal point P_{CS} and the sensing-optimal point P_{SC} . Especially for P_{SC} , we have shown that it is achieved when the transmitted waveform has a deterministic sample covariance matrix, and is modulated using the successive hypersphere coding strategy. Our analysis suggests that the essence of the S&C tradeoff may be interpreted as an information flow between Shannon and Fisher, which may shed light on the design of optimal ISAC signalling strategies.

APPENDIX A

PROOF OF PROPOSITION 2

Proof: The sensing model (2b) may be rewritten as

$$\text{vec}(\mathbf{Y}^{\text{T}}) = (\mathbf{I}_{N_s} \otimes \mathbf{X}^{\text{T}}) \text{vec}(\mathbf{H}_s^{\text{T}}) + \text{vec}(\mathbf{Z}_s^{\text{T}}). \quad (24)$$

To facilitate further derivation, we define an extended parameter vector

$$\boldsymbol{\theta} := \begin{bmatrix} (\mathbf{I}_{N_s} \otimes \mathbf{X}^{\text{T}}) \text{vec}(\mathbf{H}_s^{\text{T}}) \\ (\mathbf{I}_{N_s} \otimes \mathbf{X}^{\text{H}}) \text{vec}(\mathbf{H}_s^{\text{H}}) \end{bmatrix},$$

whose FIM can be expressed as

$$\mathbf{J}_{\boldsymbol{\theta}} = \sigma_s^{-2} \mathbf{I}_{2N_s T}. \quad (25)$$

Hence the FIM of \mathbf{h}_s is given by

$$\begin{aligned} \mathbf{J}_{\mathbf{h}_s} &= \frac{\partial \boldsymbol{\theta}}{\partial \mathbf{h}_s} \mathbf{J}_{\boldsymbol{\theta}} \left(\frac{\partial \boldsymbol{\theta}}{\partial \mathbf{h}_s} \right)^{\text{H}} \\ &= \frac{T}{\sigma_s^2} \begin{bmatrix} \mathbf{I}_{N_s} \otimes \mathbf{R}_{\mathbf{X}}^{\text{T}} & \mathbf{0} \\ \mathbf{0} & \mathbf{I}_{N_s} \otimes \mathbf{R}_{\mathbf{X}} \end{bmatrix}. \end{aligned} \quad (26)$$

Similarly, we have

$$\mathbf{J}_{\boldsymbol{\eta}} = \frac{T}{\sigma_s^2} \mathbf{F} \begin{bmatrix} \mathbf{I}_{N_s} \otimes \mathbf{R}_{\mathbf{X}}^{\text{T}} & \mathbf{0} \\ \mathbf{0} & \mathbf{I}_{N_s} \otimes \mathbf{R}_{\mathbf{X}} \end{bmatrix} \mathbf{F}^{\text{H}} \quad (27a)$$

$$= \frac{2T}{\sigma_s^2} \sum_{i=1}^{N_s} \text{Re}\{\mathbf{F}_i \mathbf{R}_{\mathbf{X}} \mathbf{F}_i^{\text{H}}\}, \quad (27b)$$

where (27b) follows from the fact that Wirtinger derivatives satisfy $(\frac{\partial}{\partial \mathbf{z}})^* = \frac{\partial}{\partial \mathbf{z}^*}$ [21]. Hence the proof is completed. \square

APPENDIX B
PROOF OF PROPOSITION 3

Proof: Rate R_1 may be expressed as

$$\begin{aligned} R_1 &= \max_{p(\mathbf{X})} I(\mathbf{Y}_c; \mathbf{X}), \text{ s.t. } \mathbf{X}\mathbf{X}^H = T\tilde{\mathbf{R}}_{\mathbf{X}}^{\text{SC}} \\ &= \max_{p(\mathbf{X})} h(\mathbf{Y}) - h(\mathbf{Y}_c|\mathbf{X}), \text{ s.t. } \mathbf{X}\mathbf{X}^H = T\tilde{\mathbf{R}}_{\mathbf{X}}^{\text{SC}}. \end{aligned} \quad (28)$$

Consider the singular value decomposition of $\mathbf{H}_c\mathbf{X}$:

$$\mathbf{H}_c\mathbf{X} = \sqrt{T}\mathbf{U}\mathbf{\Sigma}\mathbf{V}_{\text{HX}}^H. \quad (29)$$

Note that only \mathbf{V}_{HX}^H is not yet determined, since we have

$$\begin{aligned} \mathbf{G}_{\text{SC}} &= T^{-1}\mathbf{H}_c\mathbf{X}\mathbf{X}^H\mathbf{H}_c^H \\ &= \mathbf{U}\mathbf{\Sigma}\mathbf{\Sigma}^H\mathbf{U}^H, \end{aligned}$$

which is deterministic. Let us denote the first M_{SC} columns of \mathbf{U} corresponding to the non-zero singular values as $\tilde{\mathbf{U}}$. Without loss of generality, we may apply a combiner $\tilde{\mathbf{U}}^H$ at the receiver side, and obtain

$$\tilde{\mathbf{U}}^H\mathbf{Y}_c = \sqrt{T}\tilde{\mathbf{\Sigma}}\tilde{\mathbf{V}}_{\text{HX}}^H + \tilde{\mathbf{U}}^H\mathbf{Z}_c, \quad (30)$$

where $\tilde{\mathbf{U}}^H\mathbf{Z}_c \in \mathbb{C}^{M_{\text{SC}} \times T}$ has i.i.d. entries which are circularly symmetric complex Gaussian distributed, $\tilde{\mathbf{\Sigma}} \in \mathbb{C}^{M_{\text{SC}} \times M_{\text{SC}}}$ denotes the $M_{\text{SC}} \times M_{\text{SC}}$ submatrix containing non-zero singular values, and $\tilde{\mathbf{V}}_{\text{HX}}$ contains the first M_{SC} columns of \mathbf{V}_{HX} . Note that $\tilde{\mathbf{U}}^H\mathbf{Y}_c$ is a sufficient statistic of \mathbf{X} , hence the mutual information $I(\mathbf{Y}_c; \mathbf{X})$ may be expressed as

$$\begin{aligned} I(\mathbf{Y}_c; \mathbf{X}) &= I(\tilde{\mathbf{U}}^H\mathbf{Y}_c; \mathbf{X}) \\ &= h(\tilde{\mathbf{U}}^H\mathbf{Y}_c) - h(\tilde{\mathbf{U}}^H\mathbf{Y}_c|\mathbf{X}). \end{aligned} \quad (31)$$

Furthermore, we consider a projection of $\tilde{\mathbf{U}}^H\mathbf{Y}_c$ onto the space of $\mathcal{S} = \{\sqrt{T}\tilde{\mathbf{\Sigma}}\mathbf{Q}|\mathbf{Q} \in \mathbb{C}^{M_{\text{SC}} \times T}, \mathbf{Q}^H\mathbf{Q} = \mathbf{I}\}$, which may be viewed as a rescaled Stiefel manifold [22]. This can be achieved by solving the following problem

$$\tilde{\mathbf{Y}}_c := \text{Proj}_{\mathcal{S}}(\tilde{\mathbf{U}}^H\mathbf{Y}_c) = \underset{\mathbf{Y}}{\text{argmax}} \|\mathbf{Y} - \tilde{\mathbf{U}}^H\mathbf{Y}_c\|_{\mathbb{F}}^2, \text{ s.t. } \mathbf{Y} \in \mathcal{S}, \quad (32)$$

which admits a closed-form solution [22]. We note that $\tilde{\mathbf{Y}}_c$ is also a sufficient statistic of \mathbf{X} , since $\sqrt{T}\tilde{\mathbf{\Sigma}}\tilde{\mathbf{V}}_{\text{HX}}^H$ lies on the manifold \mathcal{S} and hence is not affected by the projection. Upon denoting $\tilde{\mathbf{Z}}_c = \tilde{\mathbf{Y}}_c - \sqrt{T}\tilde{\mathbf{\Sigma}}\tilde{\mathbf{V}}_{\text{HX}}^H$, we have

$$\tilde{\mathbf{Y}}_c = \sqrt{T}\tilde{\mathbf{\Sigma}}\tilde{\mathbf{V}}_{\text{HX}}^H + \tilde{\mathbf{Z}}_c. \quad (33)$$

Now the mutual information can be rewritten as

$$\begin{aligned} I(\mathbf{Y}_c; \mathbf{X}) &= I(\tilde{\mathbf{Y}}_c; \mathbf{X}) \\ &= h(\sqrt{T}\tilde{\mathbf{\Sigma}}\tilde{\mathbf{V}}_{\text{HX}}^H + \tilde{\mathbf{Z}}_c) - h(\tilde{\mathbf{Z}}_c). \end{aligned} \quad (34)$$

When $\sigma_c^2 \rightarrow 0$, the residual noise $\tilde{\mathbf{Z}}_c$ in fact distributes on the tangent space of the manifold \mathcal{S} at the point $\sqrt{T}\tilde{\mathbf{\Sigma}}\tilde{\mathbf{V}}_{\text{HX}}^H$. Note that the tangent space is an Euclidean space having a complex dimensionality of $TM_{\text{SC}} - \frac{1}{2}M_{\text{SC}}^2$. Hence the differential entropy $h(\tilde{\mathbf{Z}}_c)$ can be obtained as

$$h(\tilde{\mathbf{Z}}_c) = M_{\text{SC}}\left(T - \frac{1}{2}M_{\text{SC}}\right) \log(\pi e \sigma_c^2). \quad (35)$$

As for the term $h(\sqrt{T}\tilde{\mathbf{\Sigma}}\tilde{\mathbf{V}}_{\text{HX}}^H + \tilde{\mathbf{Z}}_c)$, let us consider the approximation

$$\begin{aligned} h(\sqrt{T}\tilde{\mathbf{\Sigma}}\tilde{\mathbf{V}}_{\text{HX}}^H + \tilde{\mathbf{Z}}_c) &= h(\sqrt{T}\tilde{\mathbf{\Sigma}}\tilde{\mathbf{V}}_{\text{HX}}^H) + \sigma_c^2 T \text{tr} \left\{ \mathbf{J}(\tilde{\mathbf{\Sigma}}\tilde{\mathbf{V}}_{\text{HX}}^H) \right\} \\ &\quad + o(\sigma_c^2), \end{aligned} \quad (36)$$

where $\mathbf{J}(\tilde{\mathbf{\Sigma}}\tilde{\mathbf{V}}_{\text{HX}}^H)$ denote the FIM of $\tilde{\mathbf{\Sigma}}\tilde{\mathbf{V}}_{\text{HX}}^H$ with respect to the distribution $p_{\tilde{\mathbf{V}}_{\text{HX}}^H}(\tilde{\mathbf{\Sigma}}\tilde{\mathbf{V}}_{\text{HX}}^H)$ itself. The approximation (36) follows from the de Bruijn identity [18, Sec. 17.7] as follows:

$$\frac{\partial}{\partial t} h(\mathbf{A} + \sqrt{t}\mathbf{N}) = \text{tr} \left\{ \mathbf{J}(\mathbf{A} + \sqrt{t}\mathbf{N}) \right\}, \quad (37)$$

where \mathbf{N} has i.i.d. zero-mean unit variance Gaussian distributed entries.

Now the remaining task is to maximize $h(\tilde{\mathbf{\Sigma}}\tilde{\mathbf{V}}_{\text{HX}}^H)$. Note that $\tilde{\mathbf{\Sigma}}\tilde{\mathbf{V}}_{\text{HX}}^H$ may be decomposed as

$$\tilde{\mathbf{\Sigma}}\tilde{\mathbf{V}}_{\text{HX}}^H = \tilde{\mathbf{\Sigma}}\mathbf{P}\mathbf{Q}, \quad (38)$$

where $\mathbf{P} \in \mathbb{R}^{M_{\text{SC}} \times M_{\text{SC}}}$ is a permutation matrix, while $\mathbf{Q} \in \mathbb{C}^{M_{\text{SC}} \times T}$ is a semi-unitary matrix satisfying $\mathbf{Q}\mathbf{Q}^H = \mathbf{I}$. Using (38), the i -th row of $\tilde{\mathbf{\Sigma}}\tilde{\mathbf{V}}_{\text{HX}}^H$ may be expressed as $\tilde{\sigma}_i \mathbf{q}_i$, where \mathbf{q}_i denotes the i -th row of \mathbf{Q} , and $\tilde{\sigma}_i$ denotes the singular value in $\tilde{\mathbf{\Sigma}}$ that multiplies on \mathbf{q}_i , which is determined by \mathbf{P} . Each $\tilde{\sigma}_i$ may take value in $\{\sigma_j\}_{j=1}^{M_{\text{SC}}}$, where σ_j represents the j -th largest singular value in $\tilde{\mathbf{\Sigma}}$. Upon denoting the probability that $\tilde{\sigma}_i = \sigma_j$ as d_{ij} , we see that the matrix \mathbf{D} whose (i, j) -th entries is d_{ij} satisfies

$$\mathbf{1}^T \mathbf{D} = \mathbf{1}^T, \quad \mathbf{D}\mathbf{1} = \mathbf{1}, \quad (39)$$

implying that \mathbf{D} is a doubly stochastic matrix.

Using the aforementioned notations, we may now express $h(\sqrt{T}\tilde{\mathbf{\Sigma}}\tilde{\mathbf{V}}_{\text{HX}}^H)$ as

$$h(\sqrt{T}\tilde{\mathbf{\Sigma}}\tilde{\mathbf{V}}_{\text{HX}}^H) = \sum_{i=1}^{M_{\text{SC}}} h(\sqrt{T}\tilde{\sigma}_i \mathbf{q}_i | \tilde{\sigma}_1 \mathbf{q}_1, \dots, \tilde{\sigma}_{i-1} \mathbf{q}_{i-1}). \quad (40)$$

Observing that $\tilde{\sigma}_i \mathbf{q}_i$ uniquely determines the pair $(\tilde{\sigma}_i, \mathbf{q}_i)$ since $\|\mathbf{q}_i\| = 1$, we obtain

$$\begin{aligned} h(\sqrt{T}\tilde{\mathbf{\Sigma}}\tilde{\mathbf{V}}_{\text{HX}}^H) &= \sum_{i=1}^{M_{\text{SC}}} h(\sqrt{T}\tilde{\sigma}_i \mathbf{q}_i | \tilde{\sigma}_{1:i-1}, \mathbf{Q}_{1:i-1}) \\ &= \sum_{i=1}^{M_{\text{SC}}} h(\sqrt{T}\tilde{\sigma}_i \mathbf{q}_i | \tilde{\sigma}_{1:i}, \mathbf{Q}_{1:i-1}) + h(\tilde{\sigma}_i | \tilde{\sigma}_{1:i-1}) \\ &= \sum_{i=1}^{M_{\text{SC}}} h(\sqrt{T}\tilde{\sigma}_i \mathbf{q}_i | \tilde{\sigma}_{1:i}, \mathbf{Q}_{1:i-1}) + h(\mathbf{P}), \end{aligned} \quad (41)$$

where $\tilde{\sigma}_{1:i} = [\tilde{\sigma}_1, \dots, \tilde{\sigma}_i]^T$, and $\mathbf{Q}_{1:i-1} = [\mathbf{q}_1^T, \dots, \mathbf{q}_{i-1}^T]^T$. Since $h(\mathbf{P})$ does not vary with SNR, in the high-SNR regime, the maximum entropy is asymptotically achieved at the maximum of $\sum_{i=1}^{M_{\text{SC}}} h(\sqrt{T}\tilde{\sigma}_i \mathbf{q}_i | \tilde{\sigma}_{1:i}, \mathbf{Q}_{1:i-1})$. Observe that

$$\begin{aligned} h(\sqrt{T}\tilde{\sigma}_1 \mathbf{q}_1 | \tilde{\sigma}_1) &= \sum_j d_{1j} h(\sqrt{T}\tilde{\sigma}_1 \mathbf{q}_1 | \tilde{\sigma}_1 = j) \\ &\leq \sum_j d_{1j} [(2T-1) \log(\sigma_j \sqrt{T}) + \log |\mathcal{S}(T, 1)|], \end{aligned} \quad (42)$$

where $[(2T-1)\log(\sigma_j\sqrt{T}) + \log|\mathcal{S}(T, 1)|]$ is the maximum entropy on the set $\{\sigma_j\mathbf{q} \mid \|\mathbf{q}\|^2 = T, \mathbf{q} \in \mathbb{C}^T\}$, corresponding to a uniform distribution on the Stiefel manifold $\mathcal{S}(T, 1)$. In general, we have

$$\begin{aligned} & h(\sqrt{T}\tilde{\sigma}_i\mathbf{q}_i \mid \tilde{\sigma}_{1:i}, \mathbf{Q}_{1:i-1}) \\ & \leq \mathbb{E}_{\tilde{\sigma}_i} \{ (2T+1-2i) \log(\sqrt{T}\tilde{\sigma}_i) + \log|\mathcal{S}(T-i+1, 1)| \} \\ & = (2T+1-2i) \log(\sqrt{T}\mathbb{E}\{\tilde{\sigma}_i\}) + \log|\mathcal{S}(T-i+1, 1)|. \end{aligned} \quad (43)$$

Now the maximization of $\sum_{i=1}^{M_{SC}} h(\sqrt{T}\tilde{\sigma}_i\mathbf{q}_i \mid \tilde{\sigma}_{1:i}, \mathbf{Q}_{1:i-1})$ amounts to

$$\begin{aligned} & \max_{\mathbf{D}} \boldsymbol{\xi}^T \mathbf{D} \mathbf{a}, \\ & \text{s.t. (39), } d_{ij} \geq 0, \forall i, j, \end{aligned} \quad (44)$$

where $\mathbf{a} = [a_1, \dots, a_{M_{SC}}]^T$ with $a_i := 2T - 1 + 2i$, while $\boldsymbol{\xi} = [\xi_1, \dots, \xi_{M_{SC}}]^T$ with $\xi_i := \log(\sqrt{T}\sigma_i)$. Observe that $\boldsymbol{\xi}^T \mathbf{D} \mathbf{a}$ is a linear function of \mathbf{D} , hence is also a matrix-convex function of \mathbf{D} . Since doubly stochastic matrices form the convex hull of permutation matrices, the optimal \mathbf{D} should be a permutation matrix, implying that the optimal \mathbf{P} should be deterministic. Given that \mathbf{P} is deterministic, the maximum $h(\tilde{\sigma}_i\mathbf{q}_i \mid \tilde{\sigma}_{1:i}, \mathbf{Q}_{1:i-1})$ can be seen to be achieved when $\tilde{\sigma}_i = \sigma_i$, meaning that

$$\begin{aligned} & \max h(\sqrt{T}\tilde{\sigma}_i\mathbf{q}_i \mid \tilde{\sigma}_{1:i}, \mathbf{Q}_{1:i-1}) \\ & = \sum_{i=1}^{M_{SC}} (2T+1-2i) \log(\sqrt{T}\sigma_i) + \log|\mathcal{S}(T-i+1, 1)|. \end{aligned} \quad (45)$$

Combining (45) and (35), we see that as $P_T/\sigma_c^2 \rightarrow \infty$, the maximum mutual information $\max I(\mathbf{Y}_c; \mathbf{X})$ is asymptotically given by

$$R_1 = \sum_{i=1}^{M_{SC}} \left(1 - \frac{2i-1}{2T}\right) \log(\lambda_i/\sigma_c^2) + c + o(1), \quad (46)$$

where

$$c = \sum_{i=1}^{M_{SC}} \left[\left(1 - \frac{2i-1}{2T}\right) \log(\pi T) - \frac{1}{T} \sum_{j=1}^{T-i} \log j \right] + M_{SC} \log 2, \quad (47)$$

which follows from the fact that $|\mathcal{S}(n, 1)| = \frac{2\pi^n}{\Gamma(n-1)}$. We note that the first term on the right hand side of (47) converges to a constant as $T \rightarrow \infty$, since for finite k we have

$$\lim_{x \rightarrow \infty} \log x - \frac{1}{x} \log \Gamma(x-k) = \lim_{x \rightarrow \infty} 1 + \log x - \psi(x-k) = 1,$$

where $\psi(x) = -\gamma - 1/x + \sum_{n=1}^{\infty} (\frac{1}{n} - \frac{1}{n+x})$ is the digamma function [23], with γ being the Euler-Mascheroni constant. Hence the proof is completed. \square

APPENDIX C

PROOF OF COROLLARY 2

Proof: Observe that $\tilde{\Sigma}\mathbf{Q}$ in (14) has an identical distribution as that of the optimal $\tilde{\Sigma}\tilde{\mathbf{V}}_{\text{HX}}^{\text{H}}$ in Appendix B that maximizes the mutual information $I(\tilde{\mathbf{U}}^{\text{H}}\mathbf{Y}_c; \mathbf{X})$ in the high-SNR regime. Hence the P_{SC} -achieving \mathbf{X} satisfies

$$\mathbf{H}_c \mathbf{X} = \sqrt{T}\tilde{\mathbf{U}}\tilde{\Sigma}\mathbf{Q}. \quad (48)$$

One of the solutions to (48) is

$$\mathbf{X} = \sqrt{T}\mathbf{H}_c^{\dagger}\tilde{\mathbf{U}}\tilde{\Sigma}\mathbf{Q}, \quad (49)$$

which completes the proof. \square

REFERENCES

- [1] F. Liu, Y. Cui, C. Masouros, J. Xu, T. X. Han, Y. C. Eldar, and S. Buzzi, "Integrated sensing and communications: Towards dual-functional wireless networks for 6G and beyond," *IEEE J. Sel. Areas Commun.*, pp. 1–1, *early access*, 2022.
- [2] Y. Cui, F. Liu, X. Jing, and J. Mu, "Integrating sensing and communications for ubiquitous IoT: Applications, trends, and challenges," *IEEE Network*, vol. 35, no. 5, pp. 158–167, Sep. 2021.
- [3] A. Liu, Z. Huang, M. Li, Y. Wan, W. Li, T. X. Han, C. Liu, R. Du, D. K. P. Tan, J. Lu, Y. Shen, F. Colone, and K. Chetty, "A survey on fundamental limits of integrated sensing and communication," *IEEE Commun. Surv. Tuts.*, pp. 1–1, *early access*, 2022.
- [4] Y. Xiong, N. Wu, Y. Shen, and M. Z. Win, "Cooperative localization in massive networks," *IEEE Trans. Inf. Theory*, vol. 68, no. 2, pp. 1237–1258, Feb. 2022.
- [5] —, "Cooperative network synchronization: Asymptotic analysis," *IEEE Trans. Signal Process.*, vol. 66, no. 3, pp. 757–772, Feb. 2018.
- [6] D. W. Bliss, "Cooperative radar and communications signaling: The estimation and information theory odd couple," in *Proc. 2014 IEEE Radar Conf.*, Covington, KY, USA, May 2014, pp. 0050–0055.
- [7] F. Liu, Y.-F. Liu, A. Li, C. Masouros, and Y. C. Eldar, "Cramér-Rao bound optimization for joint radar-communication beamforming," *IEEE Trans. Signal Process.*, vol. 70, pp. 240–253, 2022.
- [8] J. A. Zhang, F. Liu, C. Masouros, R. W. Heath, Z. Feng, L. Zheng, and A. Petropulu, "An overview of signal processing techniques for joint communication and radar sensing," *IEEE J. Sel. Top. Signal Process.*, vol. 15, no. 6, pp. 1295–1315, Nov. 2021.
- [9] F. Liu, W. Yuan, C. Masouros, and J. Yuan, "Radar-assisted predictive beamforming for vehicular links: Communication served by sensing," *IEEE Trans. Wireless Commun.*, vol. 19, no. 11, pp. 7704–7719, Nov. 2020.
- [10] W. Yuan, F. Liu, C. Masouros, J. Yuan, D. W. K. Ng, and N. González-Prelcic, "Bayesian predictive beamforming for vehicular networks: A low-overhead joint radar-communication approach," *IEEE Tran. Wireless Commun.*, vol. 20, no. 3, pp. 1442–1456, Mar. 2021.
- [11] D. Guo, S. Shamai, and S. Verdú, "Mutual information and minimum mean-square error in Gaussian channels," *IEEE Trans. Inf. Theory*, vol. 51, no. 4, pp. 1261–1282, Apr. 2005.
- [12] M. Kobayashi, G. Caire, and G. Kramer, "Joint state sensing and communication: Optimal tradeoff for a memoryless case," in *Proc. 2018 IEEE Int. Symp. Inf. Theory (ISIT)*, Vail, CO, USA, Jun. 2018, pp. 111–115.
- [13] M. Kobayashi, H. Hamad, G. Kramer, and G. Caire, "Joint state sensing and communication over memoryless multiple access channels," in *Proc. 2019 IEEE Int. Symp. Inf. Theory (ISIT)*, Paris, France, Jul. 2019, pp. 270–274.
- [14] M. Ahmadipour, M. Wigger, and M. Kobayashi, "Joint sensing and communication over memoryless broadcast channels," in *Proc. 2020 IEEE Inf. Theory Workshop (ITW)*, Virtual, Apr. 2021, pp. 1–5.
- [15] H. Joudeh and F. M. J. Willems, "Joint communication and binary state detection," *IEEE J. Sel. Areas Inf. Theory*, pp. 1–1, *early access*, 2022.
- [16] S. M. Kay, *Fundamentals of statistical signal processing: Estimation theory*, 1st ed. Prentice-Hall, Inc., 1993.
- [17] A. El Gamal and Y.-H. Kim, *Network information theory*, 1st ed. Cambridge university press, 2011.
- [18] T. M. Cover, *Elements of information theory*, 2nd ed. John Wiley & Sons, 2006.
- [19] A. Goldsmith, *Wireless communications*, 1st ed. Cambridge university press, 2005.
- [20] T. L. Marzetta, "Noncooperative cellular wireless with unlimited numbers of base station antennas," *IEEE Trans. Wireless Commun.*, vol. 9, no. 11, pp. 3590–3600, Sep. 2010.
- [21] L. Kaup and B. Kaup, *Holomorphic functions of several variables: An introduction to the fundamental theory*. Walter de Gruyter, 2011, vol. 3.
- [22] R. A. Horn and C. R. Johnson, *Matrix analysis*, 2nd ed. Cambridge university press, 2012.
- [23] D. Zwillinger and A. Jeffrey, *Table of integrals, series, and products*, 7th ed. Elsevier, 2007.